

NASA TECHNICAL  
MEMORANDUM

NASA TM X-64747

X-RAY REFLECTION EFFICIENCY OF  
NICKEL-COATED QUARTZ OPTICAL FLATS

By John M. Reynolds, Stanley A. Fields, and  
Robert M. Wilson  
Space Science Laboratory

May 10, 1973

CASE FILE  
COPY

NASA

*George C. Marshall Space Flight Center  
Marshall Space Flight Center, Alabama*

1. REPORT NO. <b>NASA TM X-64747</b>		2. GOVERNMENT ACCESSION NO.		3. RECIPIENT'S CATALOG NO.	
4. TITLE AND SUBTITLE <b>X-Ray Reflection Efficiency of Nickel-Coated Quartz Optical Flats</b>				5. REPORT DATE <b>May 10, 1973</b>	
				6. PERFORMING ORGANIZATION CODE	
7. AUTHOR(S) <b>John M. Reynolds, Stanley A. Fields, and Robert M. Wilson</b>				8. PERFORMING ORGANIZATION REPORT #	
9. PERFORMING ORGANIZATION NAME AND ADDRESS <b>George C. Marshall Space Flight Center Marshall Space Flight Center, Alabama 35812</b>				10. WORK UNIT NO.	
				11. CONTRACT OR GRANT NO.	
12. SPONSORING AGENCY NAME AND ADDRESS <b>National Aeronautics and Space Administration Washington, D. C. 20546</b>				13. TYPE OF REPORT & PERIOD COVERED <b>Technical Memorandum</b>	
				14. SPONSORING AGENCY CODE	
15. SUPPLEMENTARY NOTES <b>Prepared by Space Sciences Laboratory, Science and Engineering This report was originally issued under the same title as Marshall Space Flight Center Internal Note IN-SSL-T-69-9, dated November 28, 1969.</b>					
16. ABSTRACT <p>Results of tests to determine the reflection efficiency of quartz optical flats vacuum coated with 1000-Å nickel are presented. Of the three vacuum-coated samples tested, two had been contaminated during the firing of the Lunar Module Reaction Control System in the JSC vacuum chamber (Chamber A). Measurements were made for 1.54-, 1.79-, and 2.29-Å incident radiation. The reflection efficiency of the contaminated samples was reduced by as much as 50 percent for some angles of incidence.</p>					
17. KEY WORDS			18. DISTRIBUTION STATEMENT  <b>Unclassified - Unlimited</b> <i>John M Reynolds</i>		
19. SECURITY CLASSIF. (of this report) <b>Unclassified</b>		20. SECURITY CLASSIF. (of this page) <b>Unclassified</b>		21. NO. OF PAGES <b>25</b>	22. PRICE <b>NTIS</b>

# TABLE OF CONTENTS

	Page
INTRODUCTION . . . . .	1
INSTRUMENTATION . . . . .	1
OPTICAL SAMPLES . . . . .	5
TEST PROCEDURE . . . . .	8
RESULTS . . . . .	11
SUMMARY AND CONCLUSIONS . . . . .	14

## LIST OF ILLUSTRATIONS

Figure	Title	Page
1.	X-ray reflectometer system . . . . .	2
2.	Optical flat assembly . . . . .	4
3.	Optical samples . . . . .	5
4(A).	Vacuum coating apparatus . . . . .	6
4(B).	Vacuum coater. . . . .	7
5.	Optical bench. . . . .	8
6.	Optical slit arrangement . . . . .	10
7.	Photograph of direct and reflected X-ray beam . . . . .	11
8.	Reflection efficiency curves for quartz. . . . .	12
9.	Reflection efficiency curves for nickel. . . . .	13
10.	Reflection efficiency curves for nickel contaminated 6C2 . . . .	15
11.	Reflection efficiency curves for nickel contaminated 6C3 . . . .	16
12.	Reflection efficiency curves for nickel contaminated 6C3 at 2.29-Å radiation. . . . .	17
13.	Reflection efficiency curves at 1.54 Å . . . . .	18
14.	Reflection efficiency curves at 1.79 Å . . . . .	19
15.	Reflection efficiency curves at 2.29 Å . . . . .	20

# X-RAY REFLECTION EFFICIENCY OF NICKEL-COATED QUARTZ OPTICAL FLATS

## INTRODUCTION

During the first week of May 1969, four test beds were placed inside the MSC (Chamber A) vacuum chamber during a Lunar Module (LM) Reaction Control System (RCS) engine firing. These four test beds contained, along with other samples, quartz optical flats vacuum coated with 1000-Å nickel. There were two of these samples on each of the four test beds. Also included were four other identical test beds which served as controls during various phases of the program. G. M. Arnett and others<sup>1</sup> give a complete description of the test setup as well as results of optical measurements made on a large number of samples ranging from the near-ultraviolet through the far-infrared.

This report contains the results of tests made on the two samples contained on test bed No. 6 along with an uncoated quartz optical flat and a nickel-coated laboratory control sample. The reflection efficiency of the four samples at X-ray wavelengths of 1.54, 1.79, and 2.29 Å has been determined as a function of angle of incidence of the primary ray.

## INSTRUMENTATION

The instrumentation used for this study was an X-ray generator with associated electronics and an optical bench with various optical accessories (Fig. 1).

The X-ray generator is a standard commercial type used for X-ray diffractometry and spectrography. The generator is a constant-

---

1. Lunar Excursion Module RCS Engine Vacuum Chamber Contamination Study. MSFC, NASA TM X-53859, July 8, 1969.

potential, full-wave unit capable of voltages up to 50 kV and 50 mA. The generator table top supports an X-ray tube housing that allows quick change of the X-ray tubes.

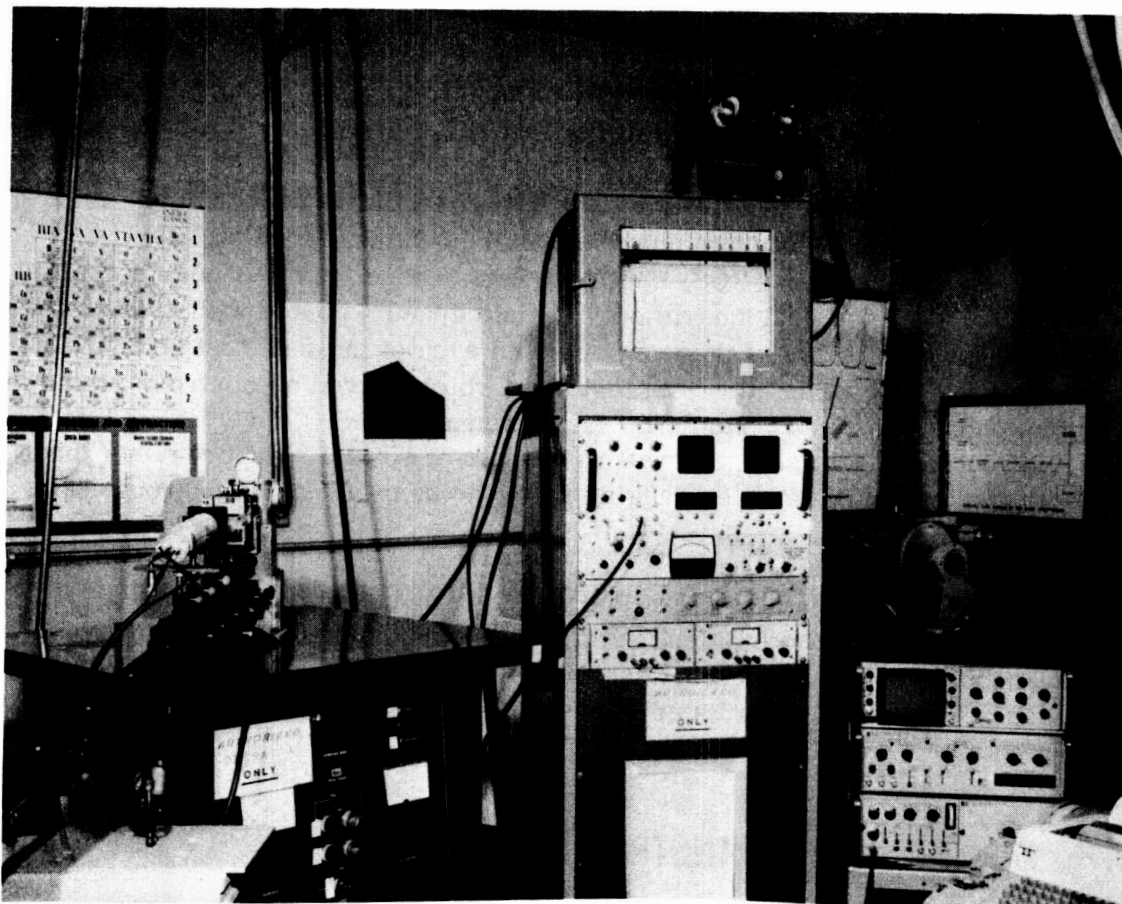


Figure 1. X-ray reflectometer system.

Standard fine-focus diffraction X-ray tubes with different target materials were used. The ones used in this study were copper, cobalt, and chromium. The  $K\alpha$  wavelength of the target materials in the X-ray tubes is as follows: Copper (Cu) 1.541 Å; Cobalt (Co) 1.789 Å; and Chromium (Cr) 2.290 Å.

For detection of X rays from these tubes, two types of radiation detectors, the scintillation counter and photographic film, were used.

The scintillation counter consists of a photomultiplier tube that has a thallium-activated sodium iodide crystal mounted in a light-tight enclosure on the window end. The X rays penetrate the beryllium window of the scintillation crystal mount and are absorbed by the thallium-activated sodium iodide crystal. The absorbed X-ray quanta cause the thallium atoms in the crystal to emit pulses of blue-violet light, the number of which is proportional to the intensity of the incident X-ray quanta. These pulses of light are transmitted through the crystal itself, through a plastic casing, and finally through the glass input window of the photomultiplier tube. Light pulses emitted by the crystal strike the photosensitive cathode of the photomultiplier tube, causing electrons to leave the cathode surface. The free electrons are accelerated toward a tube element called a dynode. The photomultiplier tube contains 10 dynodes so that the signal passing through the tube is amplified, depending on the voltage applied to the tube. After the pulses leave the scintillation detector, they are fed to an RC amplifier, to the PHA (pulse height analyzer), and then to the scaler. A rate meter is made slave to the scaler so pulses can be counted for a definite interval of time.

The other type of radiation detector is the photographic film. The camera used was the Polaroid XR-7 Land Diffraction Cassette. The cassette has a special lead-backed intensifying screen. During exposure the high-speed, high-resolution phosphor coating on the surface of the screen fluoresces, reproducing a visible light pattern of the X-ray information. The types of film used were Polaroid Polapan Type 52 and Polaroid 3000 speed Type 57.

The second major instrument used was the optical bench, which supports the optical slits, mirror assembly, and detectors.

The optical bench is mounted at right angles to the X-ray tube housing on the generator and parallel to the X-ray beam. The optical slits are mounted on the bench. These slits are used for three purposes: (1) to initially align the optical bench with the X-ray tube housing and X-ray beam; (2) to reduce the X-ray spot from the X-ray tube to a line; and (3) to block out certain portions of the X-ray beam in respect to the optical flat, optical flat assembly, and detectors.

The optical flat assembly (Fig. 2), designed on the fulcrum principle, has a micrometer at one end for small angular movements. The assembly will hold an optical flat 4 inches or smaller in diameter.

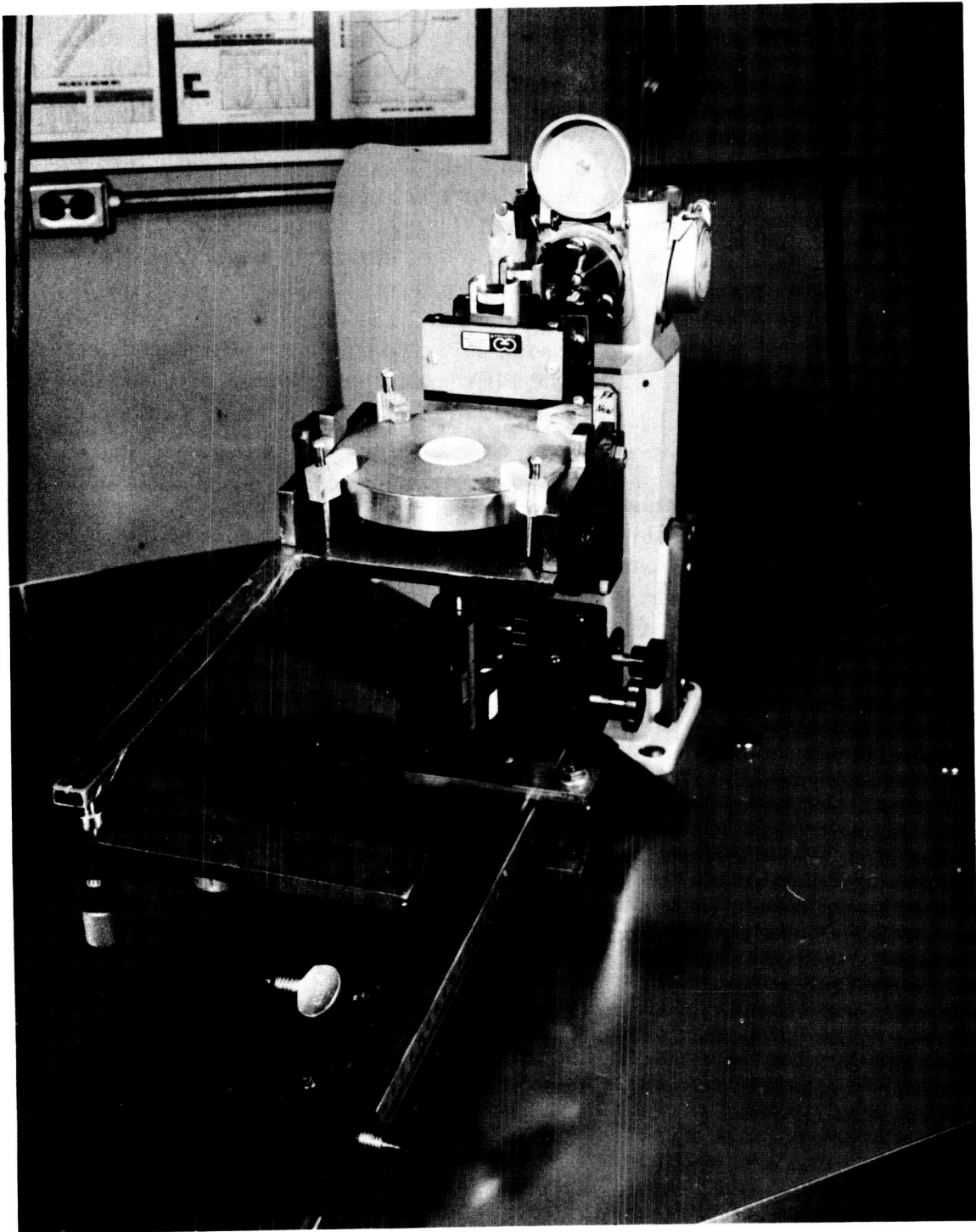


Figure 2. Optical flat assembly.

## OPTICAL SAMPLES

The samples used in this study (Fig. 3) were quartz optical flats 1 inch in diameter and one-eighth inch thick. These were tested under three conditions: (1) the clean optical flat, (2) the vacuum-coated optical flat, and (3) the contaminated vacuum-coated optical flat.

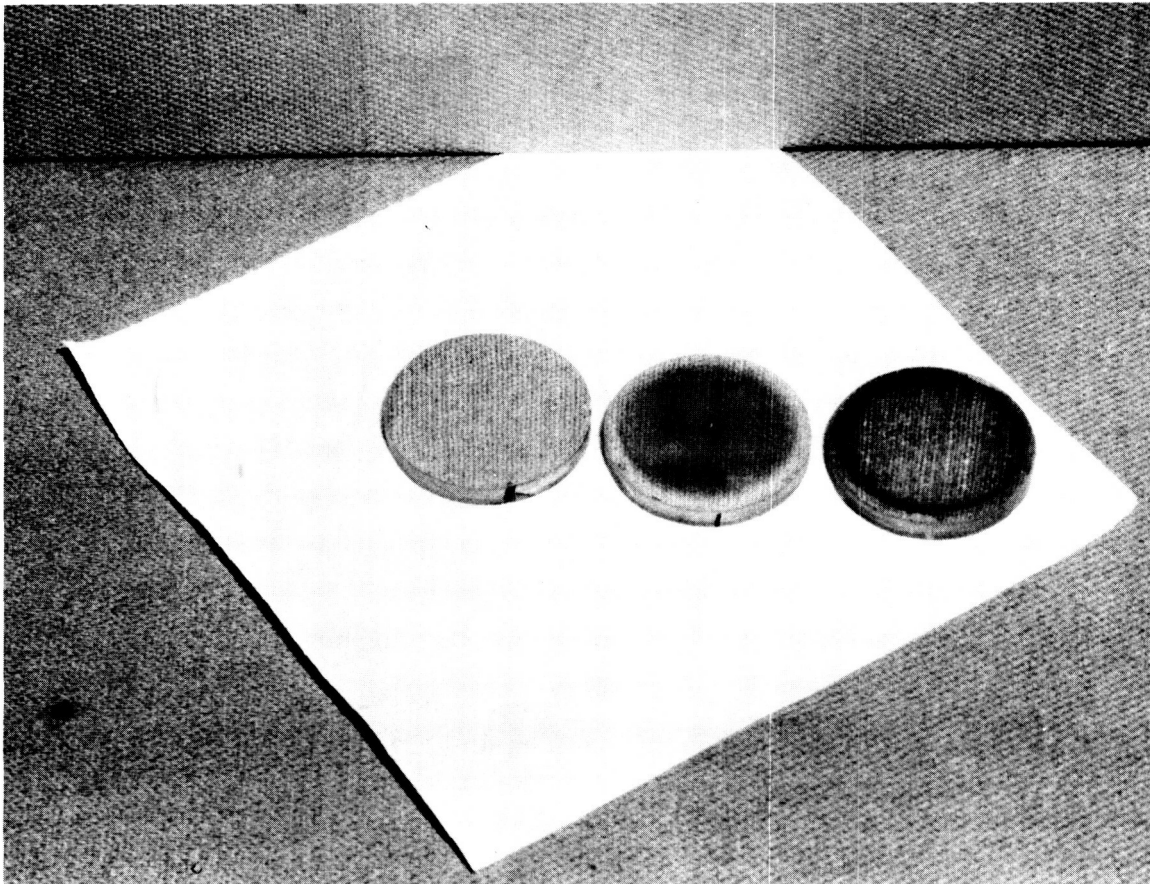


Figure 3. Optical samples.

The quartz optical flats were cleaned, dried, and placed in a circular pattern for coating with nickel. The circular array was attached to the apparatus shown in Figure 4(A) and coated with 1000 Å of nickel. The circular arrangement was selected to provide a uniform thickness of nickel on all the optical flats to be used in this test program.

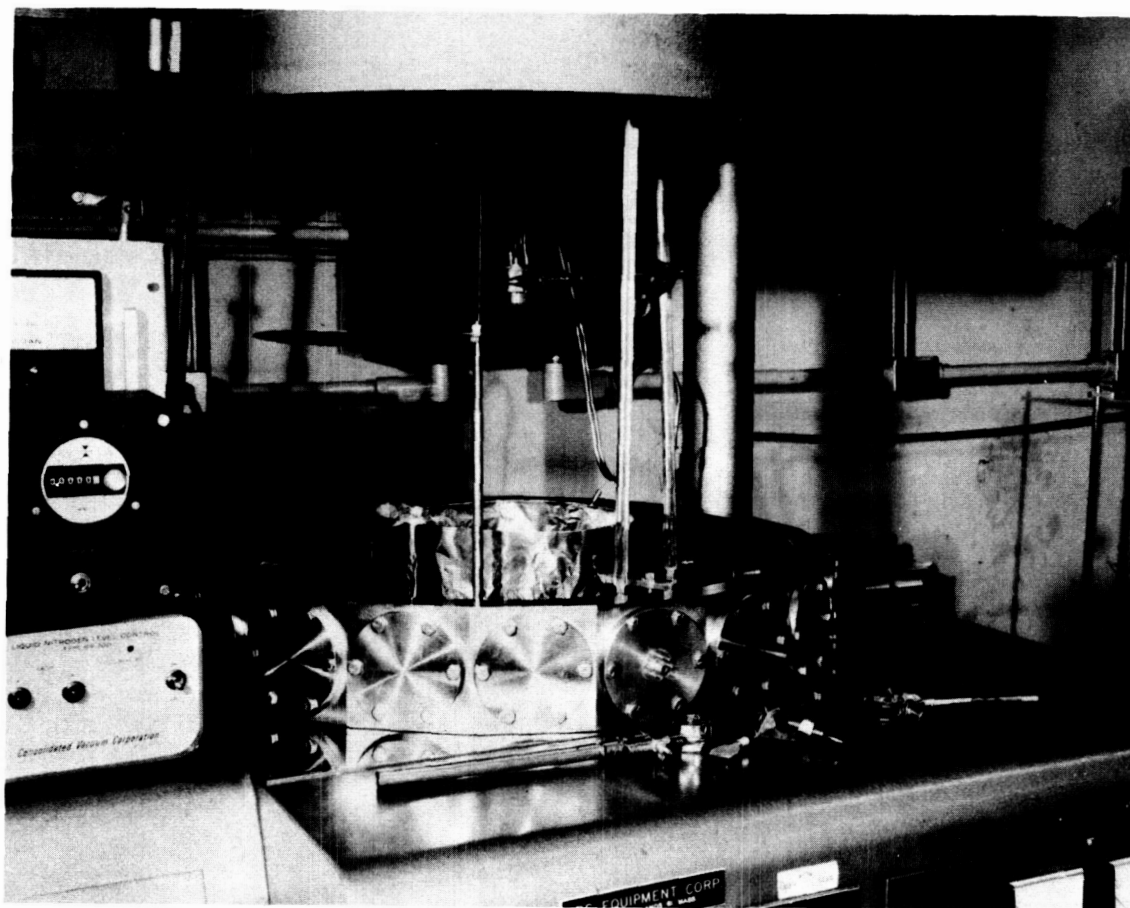


Figure 4(A). Vacuum coating Apparatus

The vacuum system used for the coating of the quartz optical flats was a silicone oil-type, self-purifying diffusion pump [ Fig. 4(B)]. Oil vapor trapping is accomplished by a circular Chevron Cryogenic cold trap. Inside the system are various terminals for different heat sources. A monitor head for measuring the thickness of the coatings was mounted in the center of the quartz optical flats. The monitor was a Sloan Quartz-Crystal Rate Monitor. Thickness of the coatings can be controlled to  $\pm 100 \text{ \AA}$ . Twenty-four of these optical flats were coated with  $1000 \text{ \AA}$  of nickel. The pressure for the vacuum-coating system during deposition ranged from  $9.0 \times 10^{-6}$  torr to  $5.0 \times 10^{-6}$  torr. The samples were removed from the vacuum coater and stored individually in glass containers with airtight lids. Sixteen of these optical flats were placed in the test beds for the LM-RCS Engine Vacuum Chamber Contamination Study. The remaining eight samples were stored in their individual containers in the laboratory at ambient temperature for individual study.

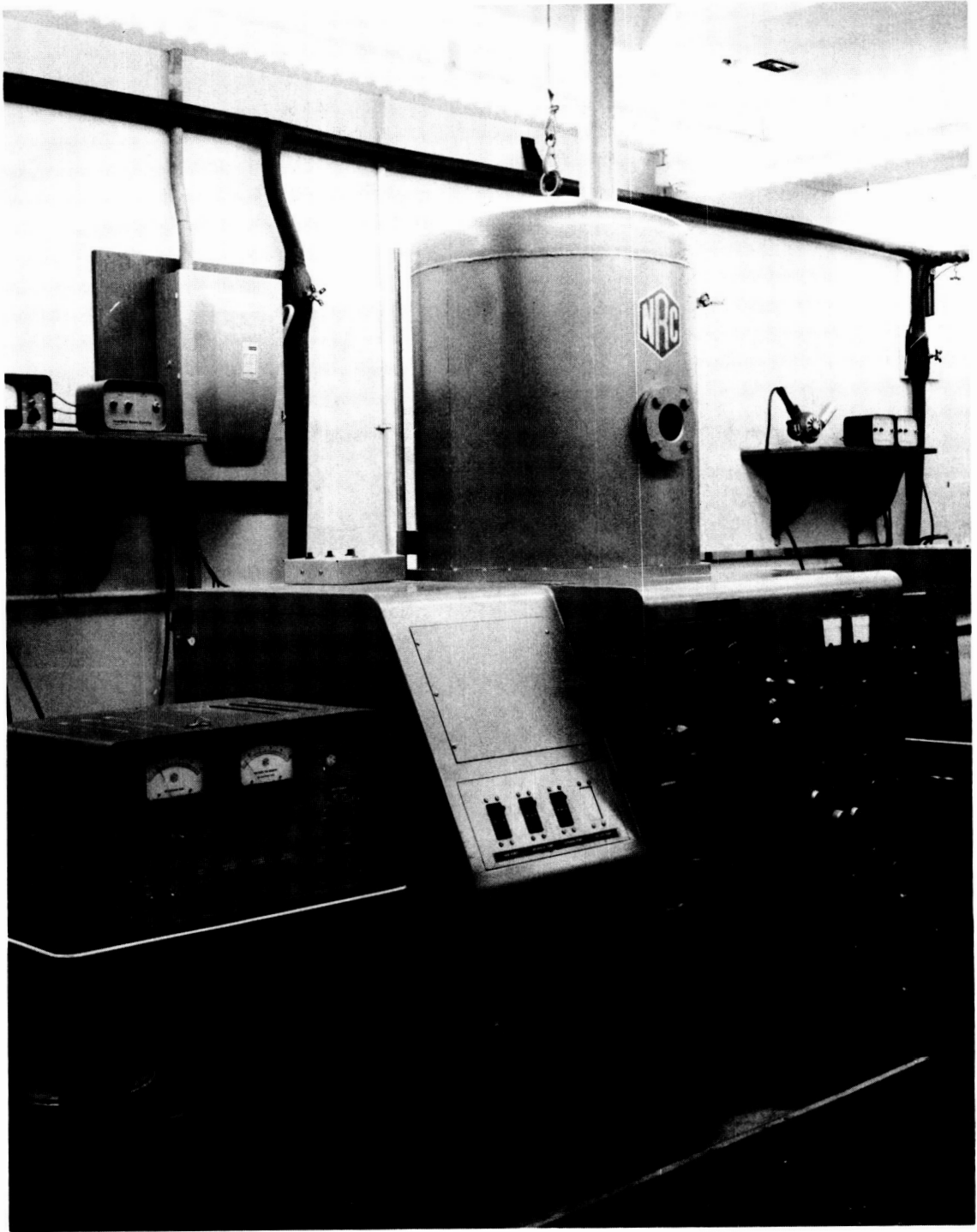


Figure 4(B). Vacuum coater.

## TEST PROCEDURE

The observation of X rays reflected from these optical flats is accomplished after the optical bench is aligned in respect to the X-ray beam and the optical flat assembly (Fig. 5). The optical bench is aligned to the X-ray

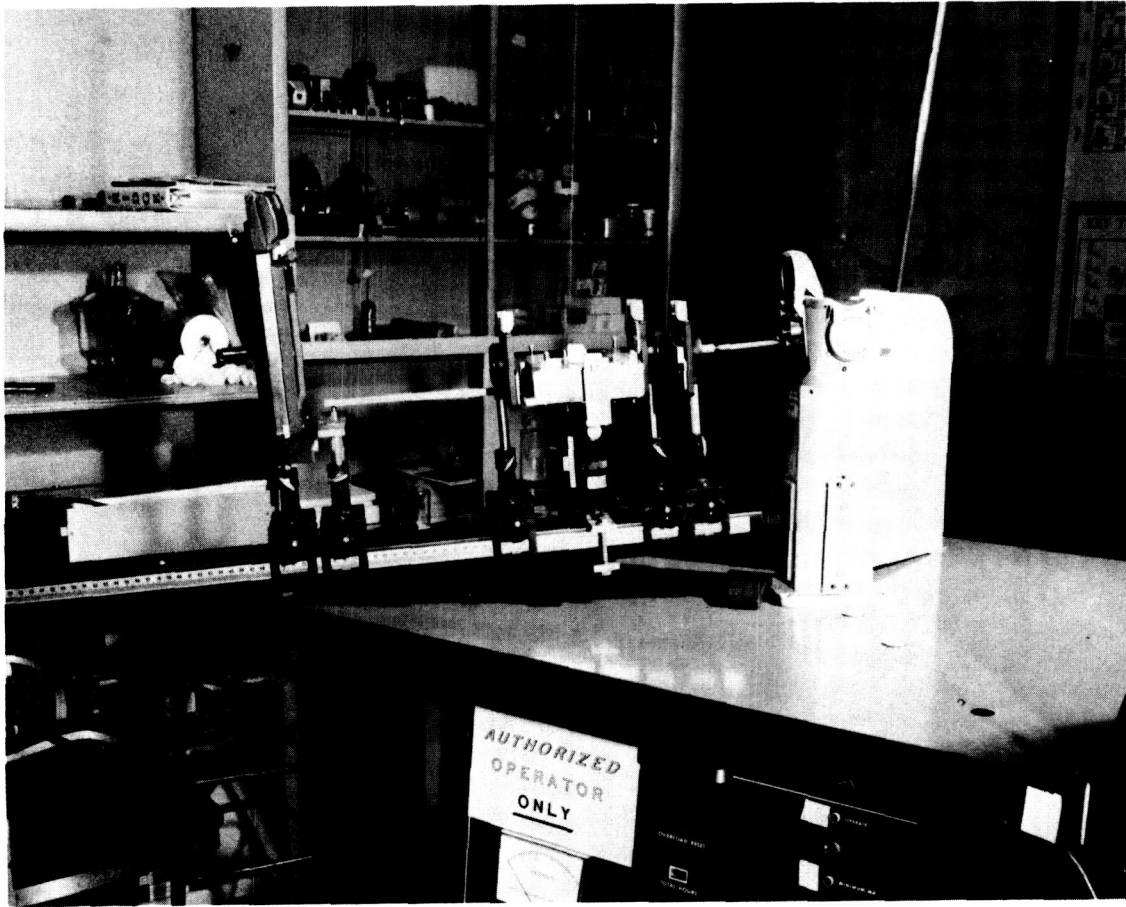


Figure 5. Optical bench.

tube tower and X-ray beam by the use of the optical slits. The first slit in the series is used to reduce the X-ray beam from circular to a line shape. The second slit is used to prevent the radiation from striking any portion of the front of the test flat. The third slit is used to block out any radiation that is not reflected by the mirror.

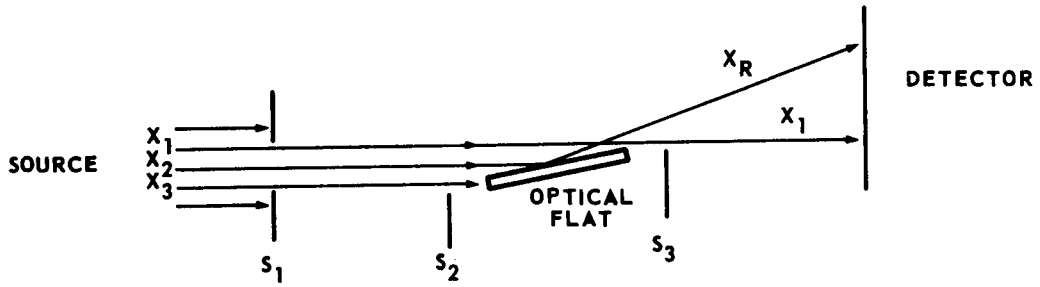
To align the X-ray beam parallel to the optical bench, the first and third slits are used without the mirror assembly. The optical slits are first brought together and positioned next to the tube tower. The third slit is closed and then opened to allow only a very small amount of line radiation to penetrate as viewed by a fluorescent screen. The third slit is then moved away from the tube tower, and the bench is adjusted so as to remain in the main X-ray beam. As the slit is moved to the extreme end of the optical bench and the bench adjusted, the X-ray beam and the optical bench become parallel.

The mirror assembly is installed on the optical bench and the slits are placed adjacent to the assembly. The mirror assembly is elevated into the X-ray beam sufficiently to allow the beam to graze the surface of the optical flat. The assembly is then adjusted such that the optical flat will be parallel to the X-ray beam.

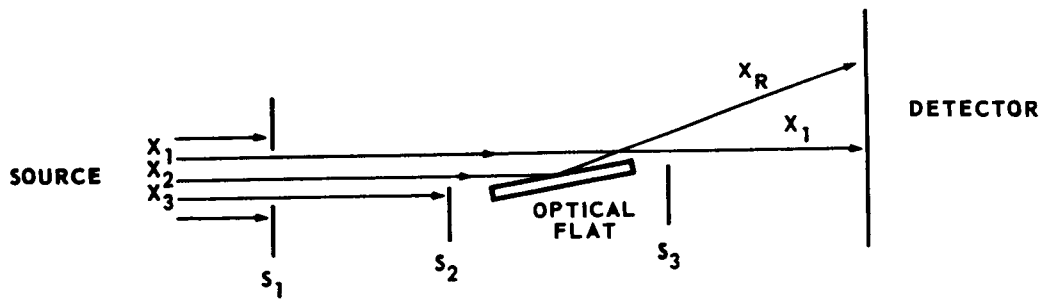
If one assumes the incident X-ray beam to be made up of a series of individual rays, then the slit arrangement can be shown as in Figure 6(A). Slit  $S_1$  is used to stop all rays from the source except  $X_1$ ,  $X_2$ , and  $X_3$ .

With the optical flat in position and the alignment complete, the micrometer is adjusted so that the optical flat makes a small angle with respect to the incident radiation. Film is used as the detector to record  $X_1$ , the direct radiation missing the optical flat, and  $X_R$ , the reflected radiation from the optical flat, (Fig. 7). This film is used to calculate the initial angle of incidence. The camera is replaced by the scintillation detector and slits  $S_2$  and  $S_3$  are adjusted. Slit  $S_2$  is raised to block out all radiation striking below the surface of the optical flat as shown in Figure 6(B).

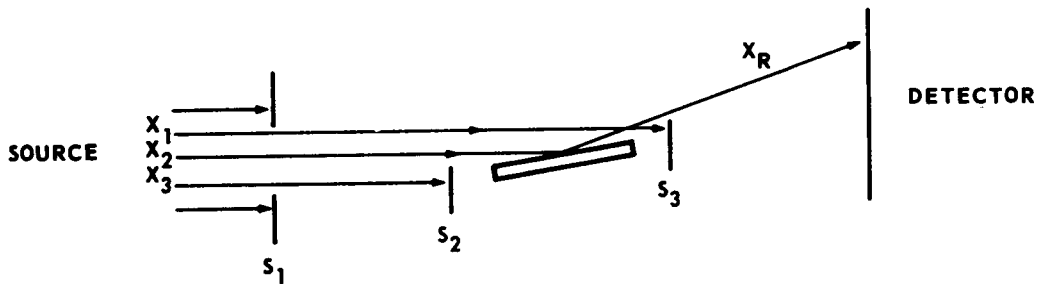
This adjustment of slit  $S_2$  is accomplished by observing the total counts received by the detector in a given interval of time with the slit out of the X-ray beam. The slit is then raised until there is a very slight decrease in total counts received. Thus no radiation is striking the front edge of the optical flat. The third slit  $S_3$  is now raised to block out  $X_1$ , the radiation missing the optical flat, so as to allow only the reflected radiation to strike the detector [Fig. 6(C)]. The correct positioning of the slits can be checked at any time by replacing the scintillation detector with the camera. The slits and optical flat are now in proper position for accumulation of X-ray reflection data.



(A)



(B)



(C)

Figure 6. Optical slit arrangement.

## RESULTS

This study determines the reflection efficiency of four test flats at three different wavelengths. The test flats shown in Figure 3 from left to right

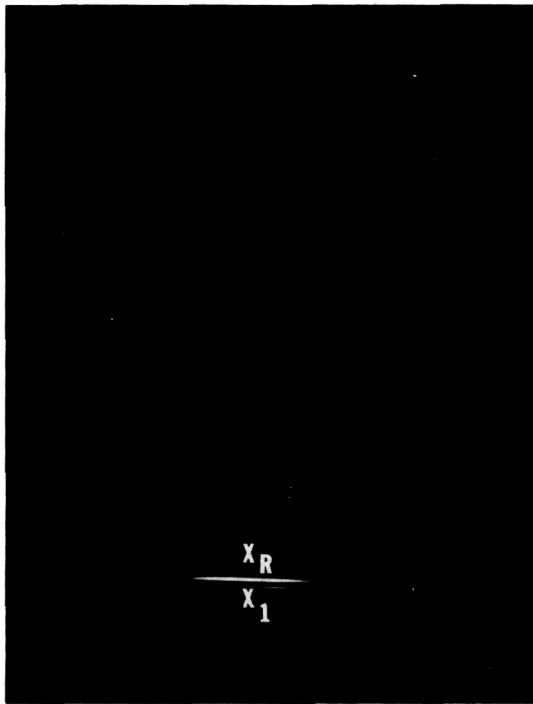


Figure 7. Photograph of direct and reflected X-ray beam.

are as follows: (1) Number 25, a quartz flat; (2) Number 17, a quartz flat vacuum-coated with 1000 Å of Ni; (3) Number 6C2, a quartz flat coated with 1000 Å of Ni and contaminated; and (4) Number 6C3, a quartz flat coated with 1000 Å of Ni and contaminated. The grid pattern which appears on the coated samples in Figure 3 is a reflection. The area of contamination on the two samples at the extreme right is the darker portion. The light area around the circumference of the sample was shielded by the test bed. The X-ray sources used in this study are as follows: (1) copper - 1.54 Å, (2) cobalt - 1.79 Å, and (3) chromium - 2.29 Å.

The reflection efficiency of the quartz flat is 95 percent, or greater, at an angle of incidence of 9 min for all three wavelengths (Fig. 8). The reflection efficiency drops off very rapidly with increased angle of incidence to 50 percent at 13.6 min

for 1.54 Å, and at 15.5 min for 1.79 Å and 2.29 Å. The reflection efficiency increases with increased wavelength, except for chromium radiation, which is less than both copper and cobalt radiation (below 12.5 min) and less than cobalt (below 15.5 min )

The reflection efficiency of the nickel-coated sample is 94 percent, or greater, at an angle of incidence of 12 min (Fig. 9). The reflection efficiency drops to 50 percent at an angle of incidence of 22.7 min for 1.54 Å, 25.4 min for 1.79 Å, and 28.5 min for 2.29 Å. The reflection again increases with increased wavelength except for chromium radiation, which is less than cobalt at angles of incidence less than 24 min.

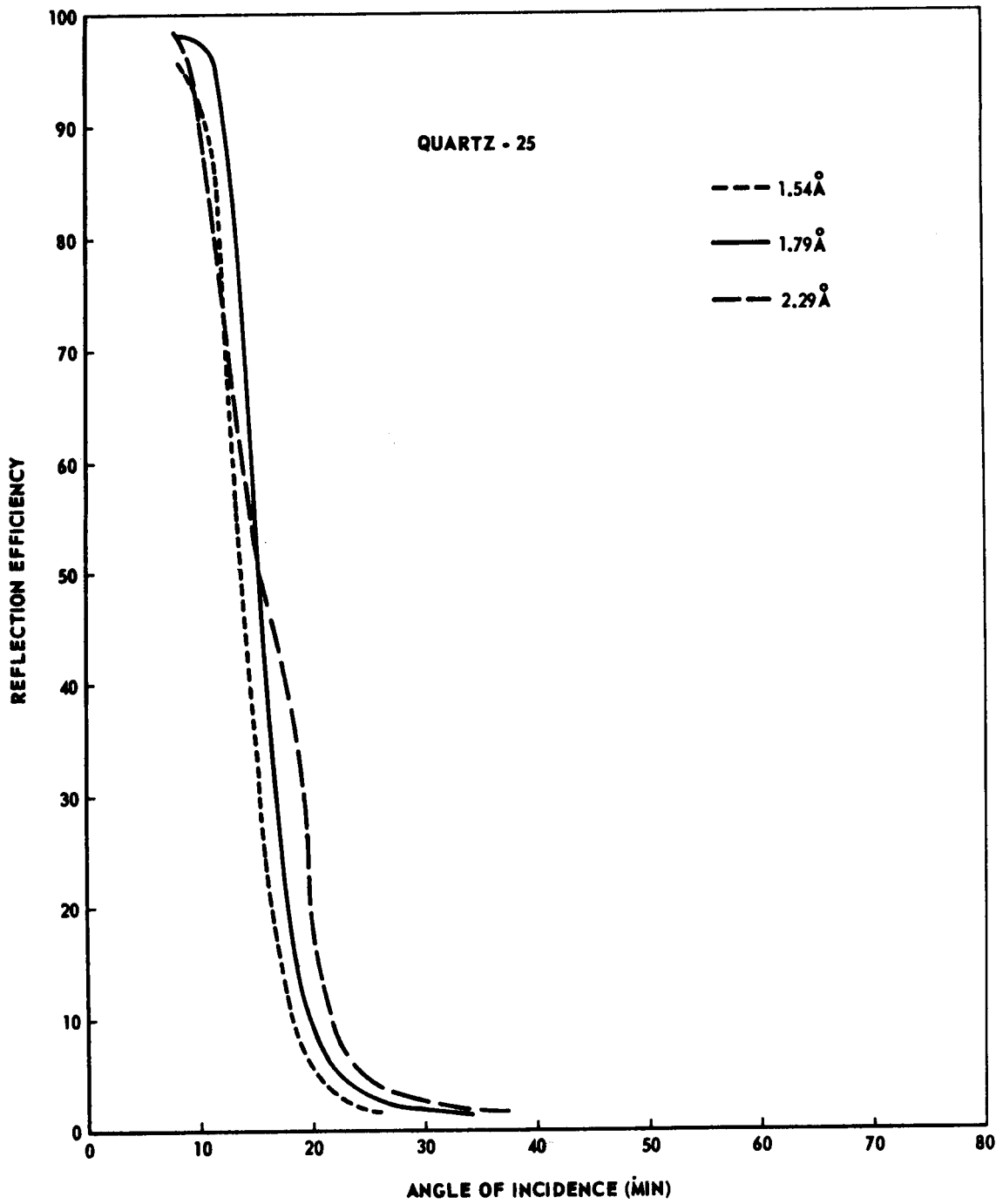


Figure 8. Reflection efficiency curves for quartz.

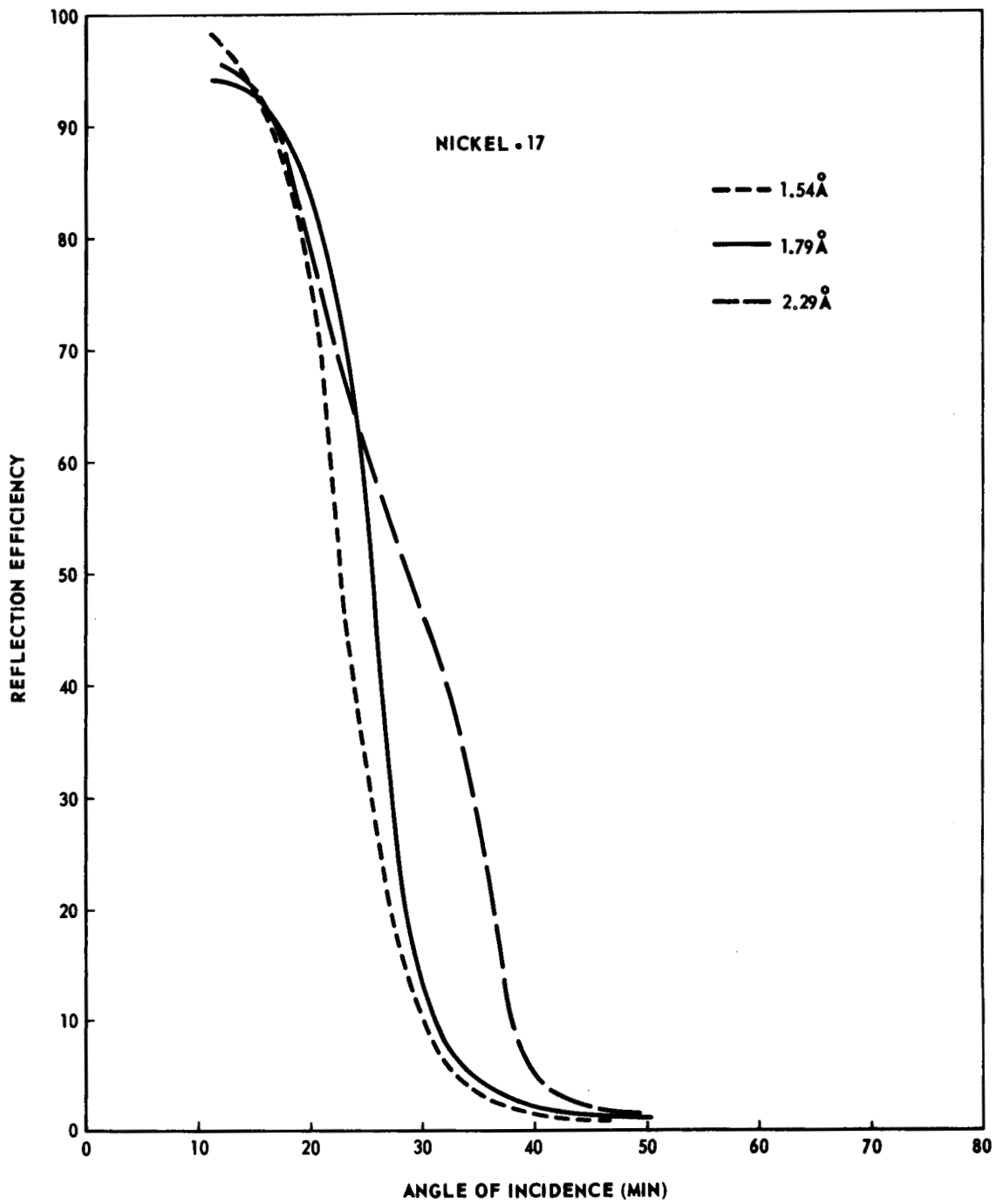


Figure 9. Reflection efficiency curves for nickel.

Figure 10 shows the results of the reflection efficiency test on contaminated sample 6C2. The reflection efficiency for all wavelength radiation was drastically reduced at small angles of incidence. At an angle of incidence of  $12 \text{ min}$  the reflection efficiency for  $1.54 \text{ \AA}$  was 47.5 percent, for  $1.79 \text{ \AA}$  was 60 percent, and for  $2.29 \text{ \AA}$  was 45 percent.

The results of the test on contaminated sample 6C3 are shown in Figure 11. Again the reflection efficiency is reduced at small angles of incidence and, as with samples 6C2, the reflection efficiency curves do not drop off rapidly as with the uncontaminated sample, but contain some discontinuities. The reflection efficiency at an angle of incidence of  $12 \text{ min}$  is 48.5 percent for  $1.54 \text{ \AA}$ , 76.5 percent for  $1.79 \text{ \AA}$ , and 64.5 percent for  $2.29 \text{ \AA}$ .

The contaminated samples 6C2 and 6C3 did not appear to be contaminated uniformly over the entire surface. To determine the effect, if any, of this visual difference, sample 6C3 was rotated through 360 degrees in 90-degree increments and the reflection efficiency at  $2.29 \text{ \AA}$  radiation was obtained. Figure 12 shows the results of this test. There was indeed a difference in the reflection efficiency of as much as 23 percent at one point.

Figures 13 through 15 show the increase in the reflection efficiency of the nickel-coated quartz flat over the uncoated quartz flat for each of the wavelengths used in this study. Also shown is the contamination effect for each wavelength.

## SUMMARY AND CONCLUSIONS

The results of the tests on the quartz flat and the nickel-coated quartz flat exhibit a high reflection efficiency at a small angle of incidence and drops off very rapidly with increased angle. The reflection efficiency for the nickel sample decreases at a slower rate than for the quartz sample. The reflection efficiency increases as the wavelength of the incidence radiation is increased for these two samples. An exception to this is the  $2.29\text{-\AA}$  radiation at small angles of incidence.

The reflection efficiency of the nickel samples was reduced by as much as 50 percent when contaminated in the LM-RCS test.

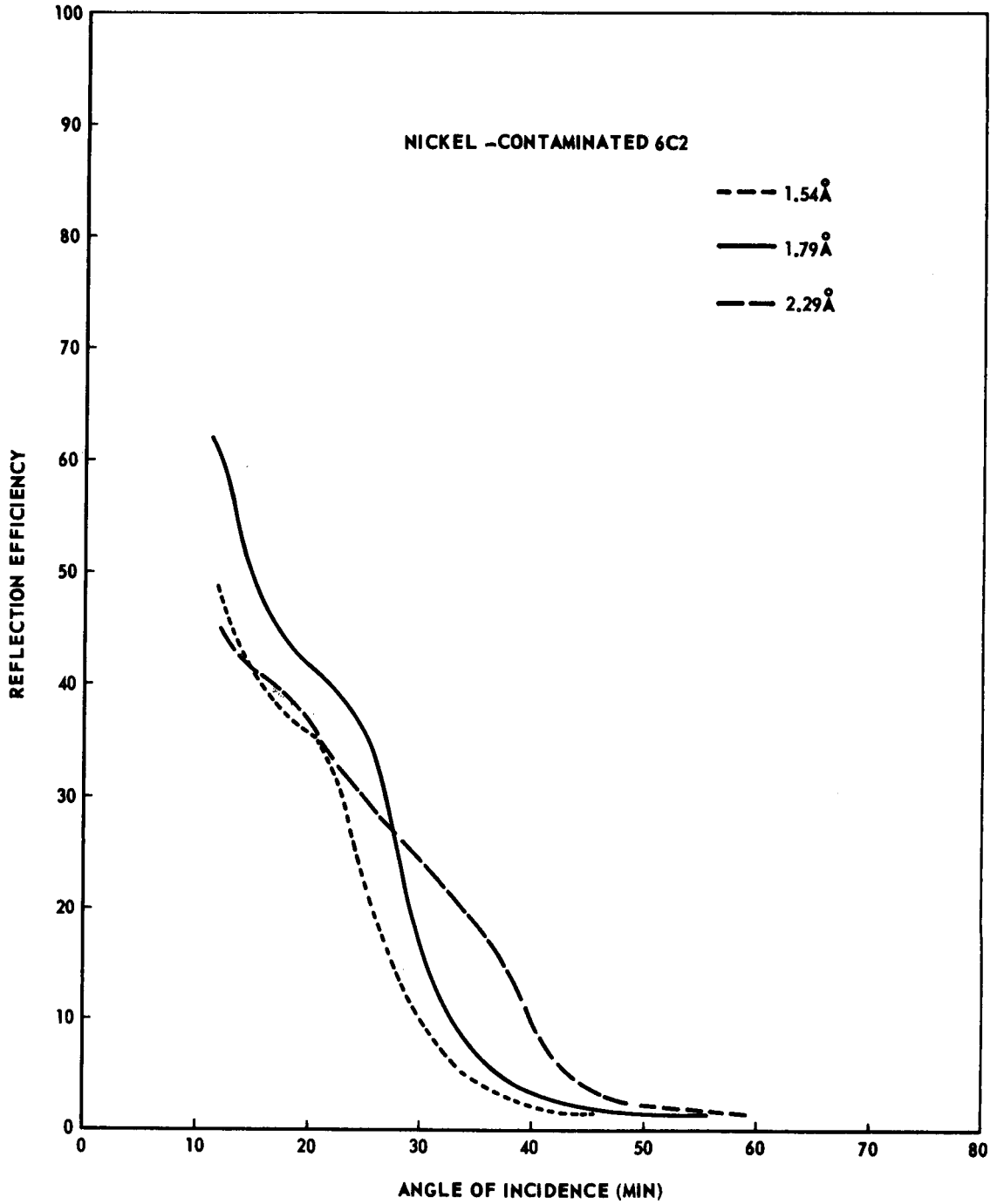


Figure 10. Reflection efficiency curves for nickel contaminated 6C2.

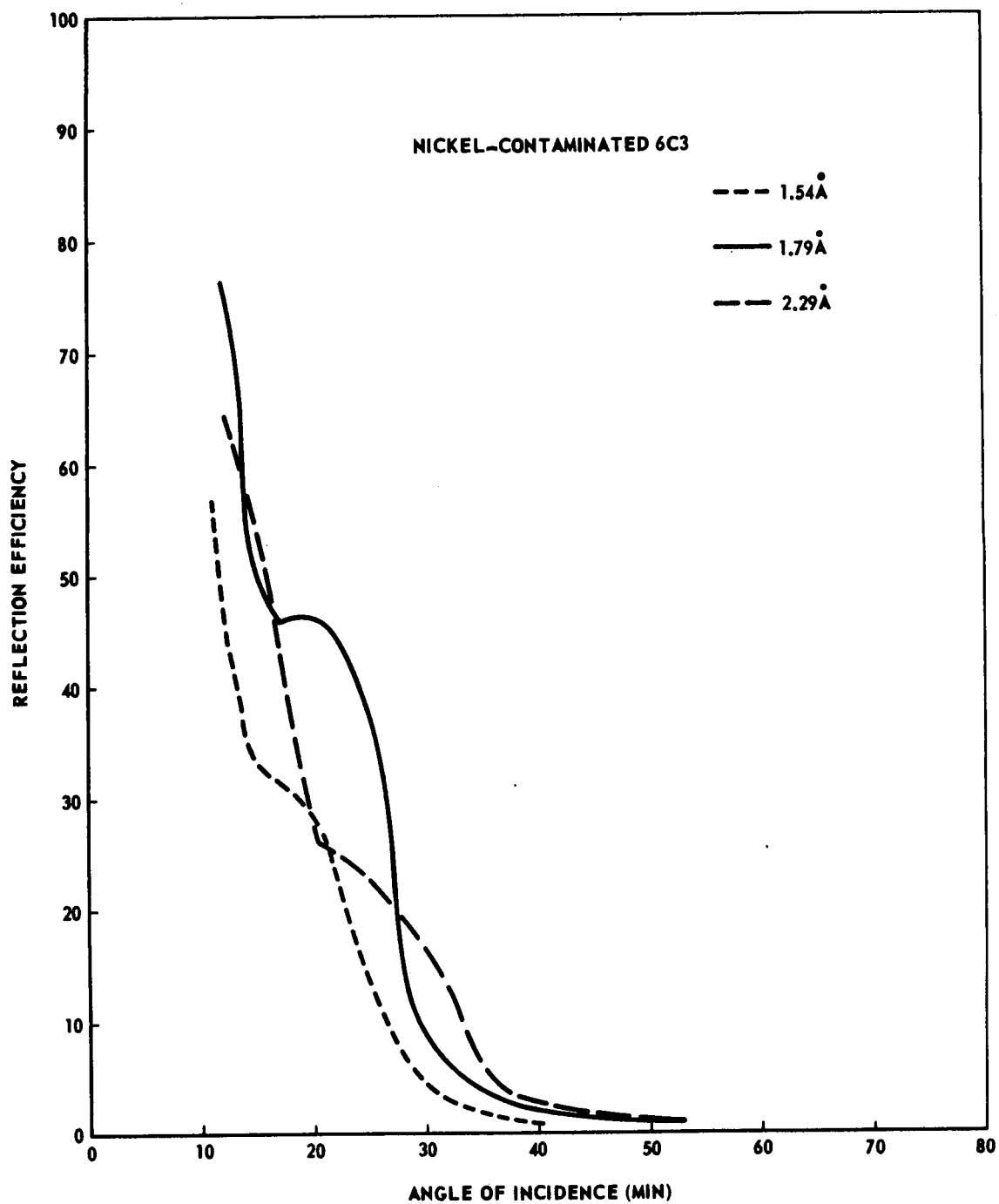


Figure 11. Reflection efficiency curves for nickel contaminated 6C3.

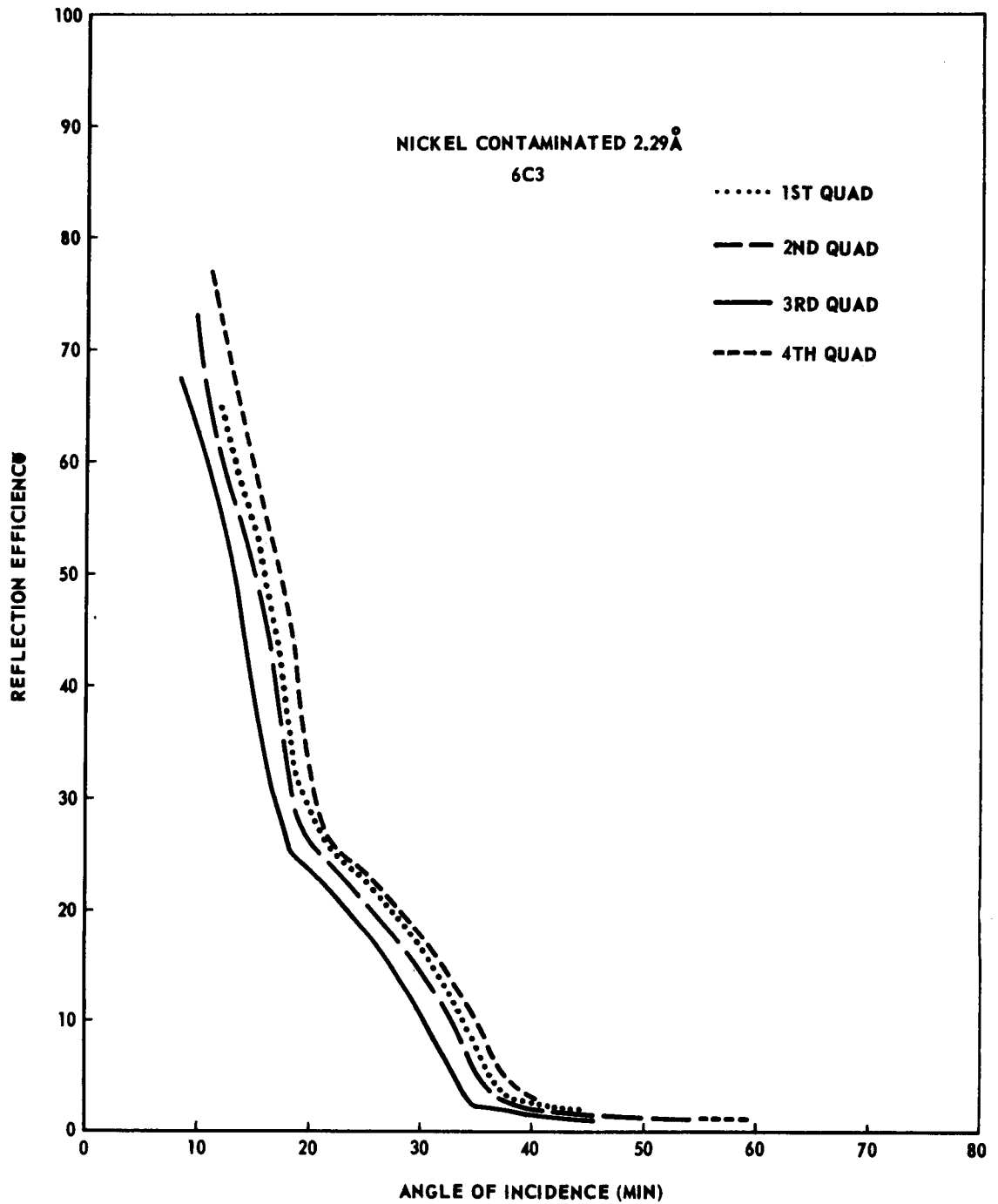


Figure 12. Reflection efficiency curves for nickel contaminated 6C3 at 2.29- $\text{\AA}$  radiation.

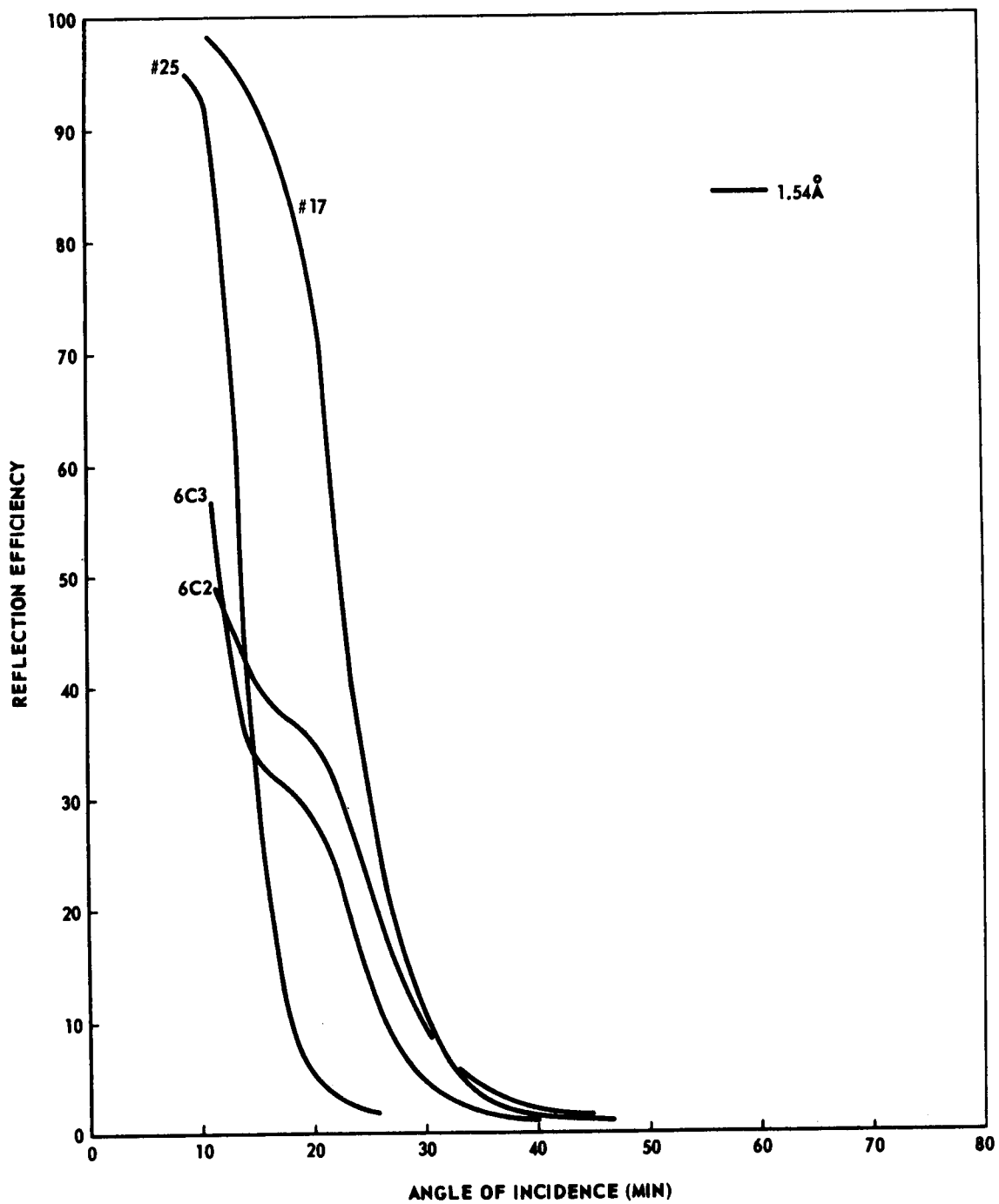


Figure 13. Reflection efficiency curves at 1.54 Å.

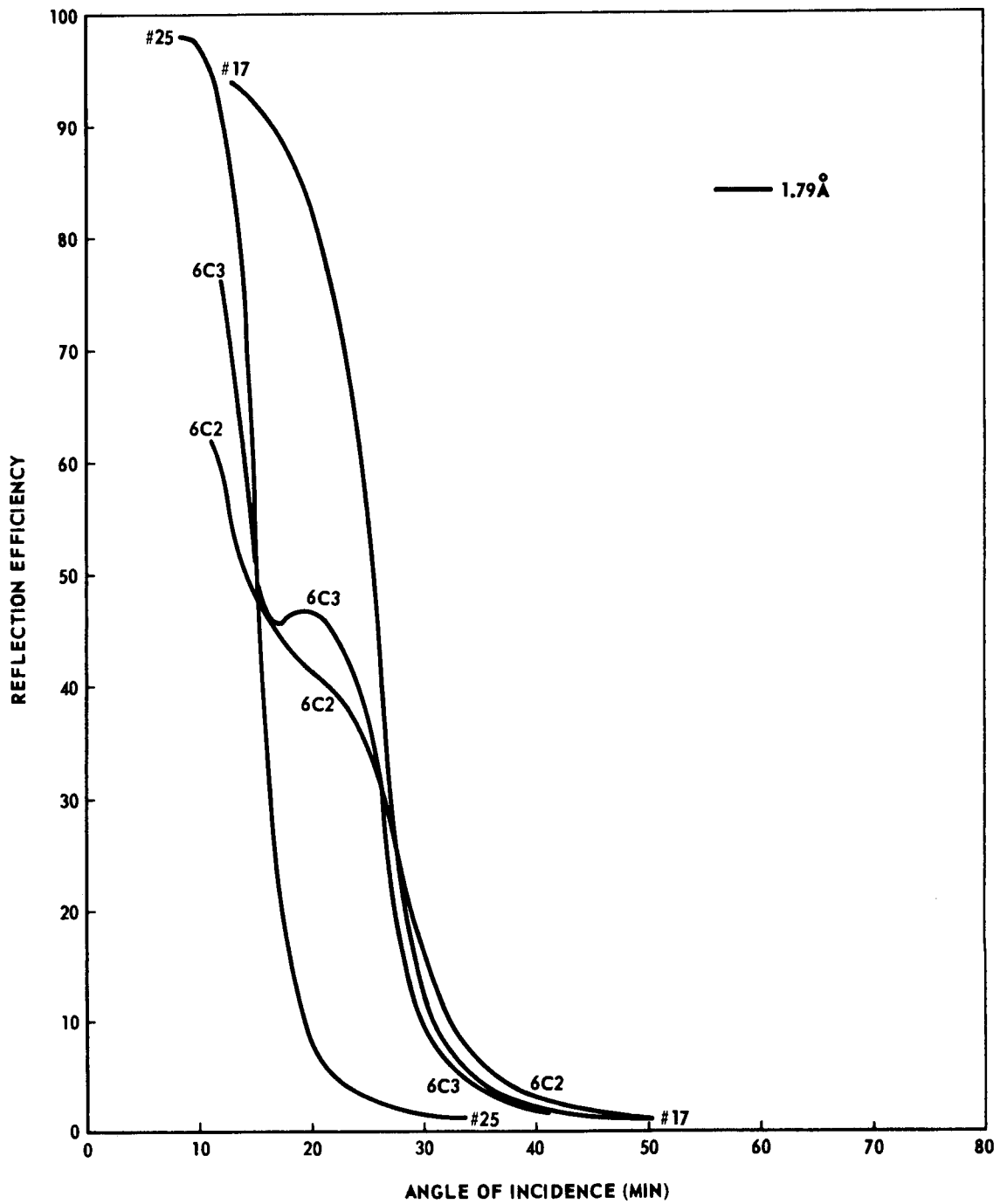


Figure 14. Reflection efficiency curves at 1.79 Å.

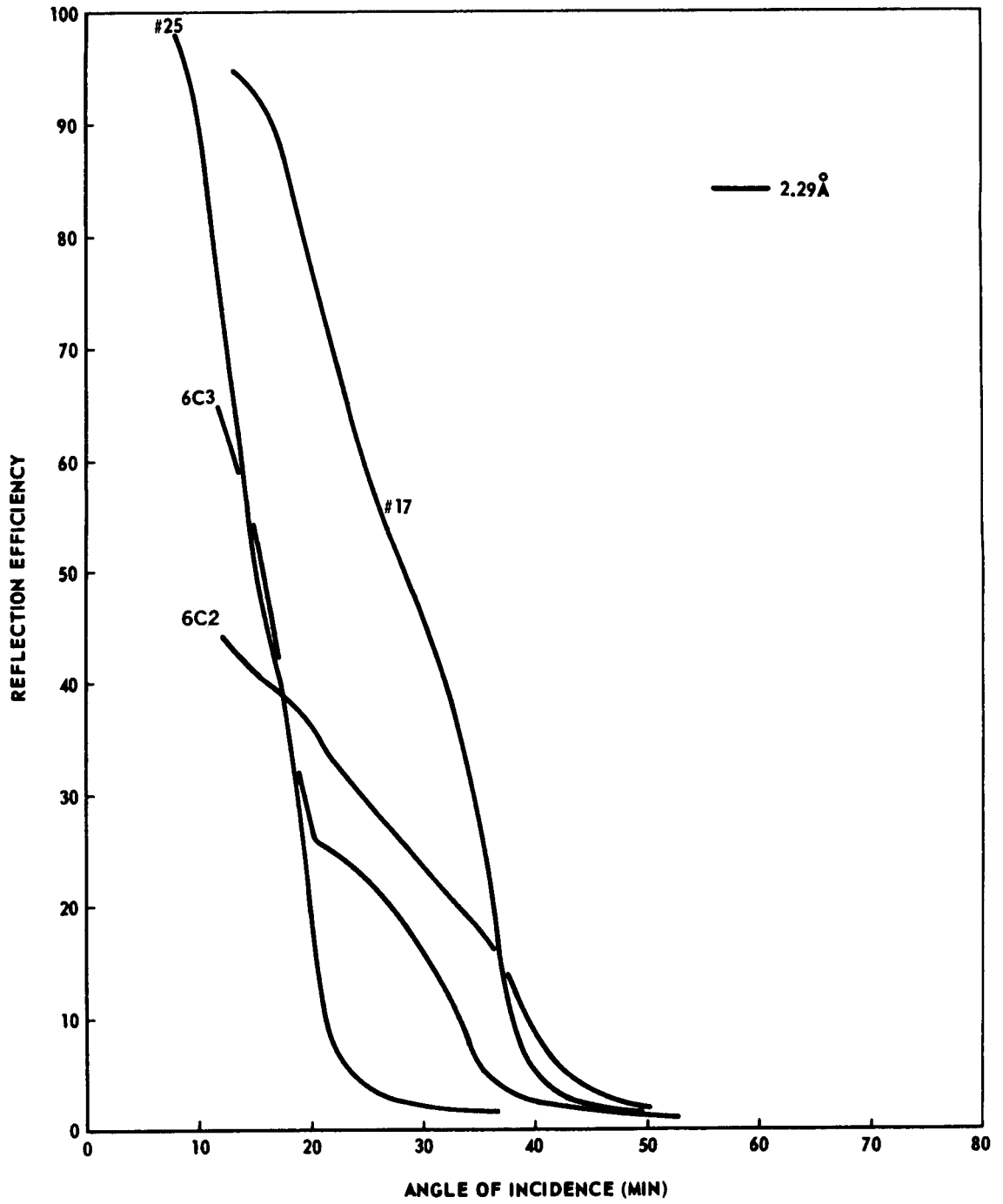


Figure 15. Reflection efficiency curves at 2.29 Å.

## APPROVAL

# X-RAY REFLECTION EFFICIENCY OF NICKEL-COATED QUARTZ OPTICAL FLATS

By John M. Reynolds, Stanley A. Fields, and  
Robert M. Wilson

The information in this report has been reviewed for security classification. Review of any information concerning Department of Defense or Atomic Energy Commission programs has been made by the MSFC Security Classification Officer. This report, in its entirety, has been determined to be unclassified.

This document has also been reviewed and approved for technical accuracy.

  
\_\_\_\_\_  
WILLIAM C. SNODDY  
Chief, Space Thermophysics Division

  
\_\_\_\_\_  
W. HAEUSSERMANN  
Acting Director, Space Sciences Laboratory

# DISTRIBUTION

## INTERNAL

### S&E-SSL-DIR

Dr. W. Haeussermann  
Mr. R. Hembree

### S&E-SSL-X

Dr. J. Dozier  
Mr. C. Winkler  
Mr. H. Weathers

### S&E-SSL-N

Dr. R. Decher

### S&E-SSL-P

Dr. R. Naumann

### S&E-SSL-S

Dr. W. Sieber

### S&E-SSL-T

Mr. W. Snoddy  
Mr. B. Jones  
Mr. E. Miller  
Mr. G. Arnett  
Mr. J. Zwiener  
Mr. J. Reynolds (10)  
Mr. S. Fields (10)  
Mr. R. Wilson (10)

### S&E-SSL-C

Reserve (5)

### A&PS-PAT

Mr. L. D. Wofford, Jr.

A&PS-MS-IP (2)

A&PS-MS-IL (8)

A&PS-MS-H

A&PS-TU (6)

## EXTERNAL

Scientific and Technical Information  
Facility (25)

P. O. Box 33

College Park, Maryland 20740

Attn: NASA Representative (S-AK/RKT)